



Geometric phaselike effects of driven transport in presence of reservoir squeezing

Javed Akhtar ¹, Jimli Goswami,^{1,2} and Himangshu Prabal Goswami ^{1,*}

¹*Department of Chemistry, Gauhati University, Jalukbari, Guwahati-781014, Assam, India*

²*Department of Civil, Construction and Environmental Engineering, North Dakota State University (NDSU), Fargo, ND 58102, USA*

 (Received 29 September 2023; revised 1 March 2024; accepted 15 April 2024; published 21 May 2024)

In a bare bosonic site coupled to two reservoirs, we explore the statistics of boson exchange in the presence of two simultaneous processes: squeezing the two reservoirs and driving the two reservoirs. The squeezing parameters compete with the geometric phaselike effect or geometricity to alter the nature of the steady-state flux and noise. The even (odd) geometric cumulants and the total minimum entropy are found to be symmetric (antisymmetric) with respect to exchanging the left and right squeezing parameters. Upon increasing the strength of the squeezing parameters, loss of geometricity is observed. Under maximum squeezing, one can recover a standard steady-state fluctuation theorem even in the presence of phase-different driving protocol. A recently proposed modified geometric thermodynamic uncertainty principle is found to be robust.

DOI: [10.1103/PhysRevE.109.054122](https://doi.org/10.1103/PhysRevE.109.054122)

I. INTRODUCTION

Phase-different multiparametric temporal driving allows an additional leverage over a system's dynamics [1,2]. This leverage is due to gauge-invariant geometric observables during the system's time evolution, which affect the driven transport and time-dependent energy conversion processes. Additional phases during the time evolution of a system that arise during cyclic variations of two parameter adiabatic driving are usually referred to as Pancharatnam-Berry phases and are known to introduce nontriviality into a well-understood system [3]. As a first application, the holonomy of the parametric space was engineered to observe bias-independent electronic pumping under slow periodic variations [4]. Subsequently, this paradigm was extended to hem in upon nonequilibrium systems that exchange matter and energy with macroscopic reservoirs [5,6]. Usually, geometric contributions in nonequilibrium quantum systems are introduced by either driving the reservoirs' temperatures or chemical potentials or even the system-reservoir couplings [6]. In such systems, the geometric effects not only actuate the steady-state dynamics but also lead to violations of the well-established fluctuation theorems (FT) and thermodynamic uncertainty relationships (TUR) [7–9], which are otherwise robust even in the presence of quantum coherences, entanglement, and quantum squeezing. These geometric effects are almost entirely quantified by identifying their contribution to the generating function describing any exchange processes in a nonequilibrium quantum system [6,9,10]. The resulting generating functions, derived from a full counting statistical (FCS) method, have an additive term apart from the inherent dynamic term, which is driving dependent and possesses a geometric curvature in the parameter space [7,11]. The geometric contribution in such nonequilibrium quantum systems can also be observed during the evolution of the system's density matrix [12]. Although

observable, it is no longer a phase factor and hence, is referred to as geometric phaselike effect or simply geometricity.

Such effects have also been explored in quantum heat engines, thermoelectric devices, and molecular junctions [12–17]. Enhancement of engine's constancy, affecting the coherent contribution to flux, observation of giant Fano factors, and fractional quantization of the flux, etc. have been reported [7,14,18]. On a separate note, in the absence of geometric effects, general observables such as flux, higher-order fluctuations, constancy, thermodynamic affinities are also affected when parameters describing the reservoirs are altered, e.g., by introducing quantum mechanical squeezing [19–25]. Squeezed reservoirs are also known to introduce additional quantum control, which have been exploited to observe nontrivial quantum thermodynamics such as additional corrective parameters on the classical fluctuation theorem of the Crooks type [26] or not leading to Jarzynski-Wojcik type of fluctuation theorem [27]. Squeezed states of the thermal reservoirs have also been exploited to overcome Carnot limit in heat engines [28–32], violate universal maximum power theories [8,14,15], and introduce higher-order correlated photon pairs from MgO:LiNbO₃ crystals [33,34]. To corral a universal understanding of the role of squeezed initial states in FTs and TURs, several possibilities are currently under conceptualization [35–37]. For example, higher-order fluctuations during photon transport can be maximized due to mixing between a qubit and squeezed resonators [38]. When treated separately, both geometricity (introduced via tuning the reservoirs) and squeezing the reservoirs inherently affect the quantum thermodynamics of nonequilibrium systems separately. Hence, it is a natural question to ask about the quantum thermodynamics of nonequilibrium systems where squeezed reservoirs are subjected to periodic modulations. This is the motivation behind this work: to simultaneously study the effect of two externally introduced reservoir processes viz. squeezing and driving on the quantum statistical thermodynamic observables. In the current work we address this question. Since presence of geometricity make even a simple model, e.g., a

*hpg@gauhati.ac.in

resonant level coupled to two thermal or electronic reservoirs, nontrivial [12,17], we focus on such a system, where the reservoirs are squeezed.

In this work, we study the effect of squeezing the reservoirs on the statistics of particle exchange when the temperature of the reservoirs are periodically modulated. The geometricity that manifests itself into the quantum statistics is explored in a toy model, which is a bare site coupled to two squeezed reservoirs. Such a model is passably standard and well studied in quantum transport [7,39,40]. Our work focuses on identifying the competition between squeezing and driving on the fluctuations of boson exchange within a quantum statistical framework. We implement the acknowledged methodology of full counting statistics (FCS) within a quantum master equation framework [41]. First, in Sec. II we present our model and the general formalism used. In Sec. III, we show our results and analysis after which we conclude in Sec. V.

II. MODEL AND FORMALISM

A bare site coupled to two reservoirs has been thoroughly studied both in presence and absence of squeezing [24,42–44]. The site can be effectively described by two Fock states that correspond to a boson-occupied ($|1\rangle$) and an unoccupied state, ($|0\rangle$), separated by an energy $\hbar\omega_o$ (see the Appendix for the Hamiltonian). Such approximations work well at relatively low temperatures with some nonlinear effect that drastically increases the energy level of the two occupied state. Therefore, higher occupied states in this situation can be neglected. On the experimental front, such a model can be a flexural mode of a GaAs-based nanobeam structure piezoelectrically coupled to squeezed electronic noise (squeezed thermal reservoirs) [31] or a qubit system realizable in an NMR setup [45] as well as in a transmon qubit around a SQUID setup [46]. The schematic representation of the model is shown in Fig. 1(a). In such a nonequilibrium system, the time evolution of reduced density matrix, $\hat{\rho}$, (within standard Born-Markov approximation techniques) is a Pauli rate equation (decoupled from coherences) with two Fock states, $|1\rangle$ and $|0\rangle$ acting as the boson exchanger between the two squeezed reservoirs. When the reservoirs are driven, the rates become time dependent (see the Appendix). Within the standard theory of full counting statistical (FCS) formalism [41,47], one can keep track of the net number of bosons exchanged, q , through a moment generating vector for the reduced system in terms of the auxiliary counting field, λ . In the Liouville space, the reduced moment generating density vector, $|\check{\rho}(\lambda, t)\rangle$, can be written as,

$$|\check{\rho}(\lambda, t)\rangle = \check{\mathcal{L}}(\lambda, t)|\check{\rho}(0, 0)\rangle, \quad (1)$$

where the elements of the density vector contains the populations of the occupied and unoccupied states, $\{\rho_{11}, \rho_{00}\}$ (Appendix) with the time-dependent evolution superoperator, $\check{\mathcal{L}}(\lambda, t)$, given by

$$\check{\mathcal{L}}(\lambda, t) = \begin{bmatrix} -\alpha_L(t) - \alpha_R(t) & \beta_L(t)e^\lambda + \beta_R(t) \\ \alpha_L(t)e^{-\lambda} + \alpha_R(t) & -\beta_L(t) - \beta_R(t) \end{bmatrix}. \quad (2)$$

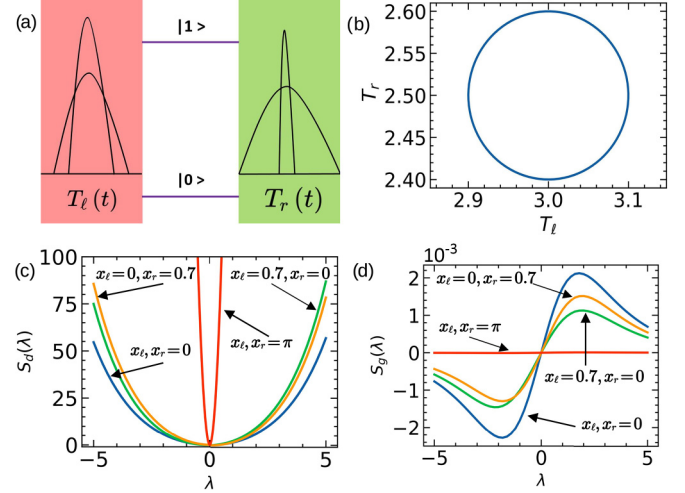


FIG. 1. (a) Schematic diagram of two squeezed harmonic baths interacting with a bosonic site with two Fock states ($|0\rangle$ and $|1\rangle$). The temperatures of the two squeezed baths are time dependent via an amplitude-modulated phase-different driving protocol as per Eq. (5) and (b) represents a circle in the parameter space of T_ℓ and T_r with $T_\ell^o = 3$, $T_r^o = 2.5$. Squeezing dependent (c) dynamic (d) geometric cumulant generating function with squeezing parameters $(x_\ell, x_r) = (0,0)$, $(0.7,0)$, $(0,0.7)$, and (π, π) for (c) outermost to innermost curves and (d) in order of decreasing magnitude. The other parameters are fixed throughout the paper at $\omega_o = 1$, $\gamma_\ell = \gamma_r = 1$, $\Omega = 150$, $A_o = 0.1$, $\phi = \pi/4$ in natural unit system ($\hbar \rightarrow 1$, $k_B \rightarrow 1$).

It is a standard practice to ignore the Lamb shifts terms so that the quantum mechanical rates of boson exchange between the system and reservoirs can be recast as:

$$\alpha_\nu(t) = \gamma_\nu \left\{ \cosh(2x_\nu) \left(n_\nu(t) + \frac{1}{2} \right) + \frac{1}{2} \right\}, \quad (3)$$

$$\beta_\nu(t) = \gamma_\nu \left\{ \cosh(2x_\nu) \left(n_\nu(t) + \frac{1}{2} \right) - \frac{1}{2} \right\}. \quad (4)$$

γ_ν , $\nu = \ell, r$ represents the coupling of the bare site and the ν th reservoir with $n_\nu = (e^{\hbar\omega_o/T_\nu(t)} - 1)^{-1}$ being the Bose-Einstein distribution of the ν th bath. $x_\nu > 0$ is the renormalized parameter responsible for squeezing the ν th harmonic bath within the Markovian regime [48] (see the Appendix). Within this approximation, the squeezing properties get symmetrically distributed about the concerned left or right squeezed bath's frequency [49]. The parametric modulation is present in the reservoirs' temperatures, $T_\nu(t)$, which we take to be of the following form,

$$T_\ell(t) := T_\ell^o + A_o \cos(\Omega t + \phi), \quad (5)$$

$$T_r(t) := T_r^o + A_o \sin(\Omega t + \phi), \quad (6)$$

A_o , Ω , and ϕ are the amplitude, frequency, and phase difference between the driving protocols, respectively. Note that this theory is valid under the adiabatic evolution assumption, where the individual decay timescales of the system and reservoirs are well separated, i.e., $t_B \ll t_s \ll t_d$, where t_d , t_B , and t_s correspond to driving, bath, and system correlation times, respectively (see the Appendix). Bosonic baths have been realized recently in an ^{87}Rb cold atomic heat engine

through probe and coupling lasers using principles from electromagnetically induced transparency [50]. By driving the Rabi frequencies of such probe and coupling lasers through an appropriately constructed time-dependent protocol one can, in principle, perhaps achieve leverage over the reservoir temperature modulations. A schematic representation of the temperature driving that leads to a circle is shown in Fig. 1(b).

In the steady state, when $\lambda = 0$, a zero eigenvalue $\zeta_o(t)$ is obtained from the right-hand side (RHS) of Eq. (2). From this zero eigenvalue, a cumulant generating function, $S(\lambda)$ within the domain $\lambda \in \{-\infty, \infty\}$, can be constructed, which allows evaluation of the n th-order cumulants, $j^{(n)} = \partial_\lambda^n S(\lambda)|_{\lambda=0}$ [41]. In the presence of phase-different driving protocol, $S(\lambda)$ is known to be additively separable into two components, one dynamic [$S_d(\lambda)$], and a geometric term $S_g(\lambda)$, which are both cumulant generating functions: dynamic cumulant generating functions and the other is geometric cumulant generating functions, respectively. The geometric term or geometric cumulant generating function, $S_g(\lambda)$ essentially is the source of geometricity in such driven dynamics and is obtainable from the left eigenvector ($\langle L_o(\lambda, t) |$) and the right eigenvector ($|R_o(\lambda, t)\rangle$) of the RHS of Eq. (1) for the eigenvalue $\zeta_o(\lambda, t)$. It is nonexistent if the two parameters [Eq. (5)] are driven without any phase difference, i.e., $\phi = 0$ [17]. Both $S_d(\lambda)$ and $S_g(\lambda)$ as a function of the counting field is depicted in Figs. 1(c), 1(d) for different values of squeezing parameters x_ℓ and x_r . As the reservoirs' squeezing is increased, the dynamic cumulant generating function also gets squeezed making it a sharper convex downward function [see the innermost curve in Fig. 1(c), where $x_\ell = x_r = \pi$]. This behavior is not different than what was earlier observed for the nondriven scenario [51]. For the geometric cumulant generating function, $S_g(\lambda)$, Fig. 1(d), an increased squeezing starts to reduce the amplitude of the function finally making it zero at high values (see the flat line where $x_\ell = x_r = \pi$). Thus at high squeezing of reservoirs, one will not see any geometric effects. We explore this latter aspect in detail in later parts of the work.

Both the dynamic and geometric cumulants can be evaluated as [7,7–12]

$$j_d^{(n)} = \partial_\lambda^n S_d(\lambda)|_{\lambda=0} = \frac{1}{t_p} \int_0^{t_p} \partial_\lambda^n \zeta_o(\lambda, t)|_{\lambda=0}(t) dt \quad (7)$$

$$j_g^{(n)} = \partial_\lambda^n S_g(\lambda)|_{\lambda=0} = \frac{1}{t_p} \int_0^{t_p} \partial_\lambda^n \langle L_o(\lambda, t) | \dot{R}_o(\lambda, t) \rangle dt |_{\lambda=0} \quad (8)$$

$$= -\partial_\lambda^n \left(\iint_S \mathcal{F}_{T_\ell T_r}(\lambda) dT_\ell dT_r \right) |_{\lambda=0} \quad (9)$$

with $t_p = 2\pi/\Omega$ being the time period of the chosen external driving [Eq. (5)]. In Eq. (9), the integrand, $\mathcal{F}_{T_\ell T_r}(\lambda)$, is known as the geometric curvature and is analogous to the Pancharatnam-Berry curvature [7,7–12] in the T_ℓ, T_r surface, S . Here, $n = 1$ and 2 correspond to the flux and noise, respectively. Both the quantities depend on the squeezing parameters, x_ℓ, x_r through the modified rates in Eq. (3) and Eq. (4). The dynamic and geometric cumulant generating functions are shown in Figs. 1(c), 1(d) for different squeezing parameters.

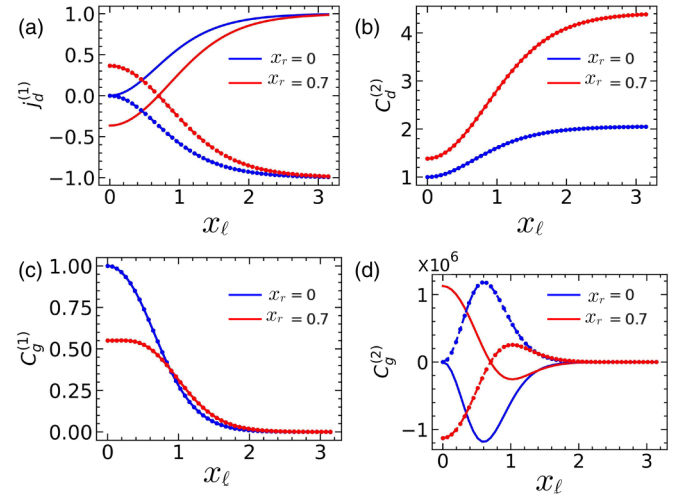


FIG. 2. (a) Behavior of the absolute dynamic flux, $j_d^{(1)}$ as a function of the two reservoirs' squeezing parameters evaluated at equal initial temperatures $T_\ell^o = T_r^o = 3$. The solid (dotted) lines are when x_r is fixed at 0 and 0.7 and x_ℓ is varied [x_ℓ and x_r are exchanged in Eq. (7)]. Note the antisymmetry due to exchange between x_ℓ and x_r . (b) Behavior of the scaled dynamic noise (second cumulant). Note the equality upon exchanging the x_ℓ and x_r values. Plot of geometric scaled flux (c) and noise (d) highlighting the equality and antisymmetry upon exchanging the squeezing parameters.

III. RESULTS AND DISCUSSION

By evaluating the eigensystem of Eq. (2), we can identify the smallest eigenvalue $\zeta_o(\lambda, t)$ [see the Appendix, Eq. (A14)], from which we numerically obtain the dynamic flux and noise using Eq. (7). The time integrals in Eq. (7) and Eq. (8) cannot be performed analytically up to complete closure. Further, only the curvature $\mathcal{F}_{T_\ell T_r}(\lambda)$ can be known analytically for the considered system (discussed later), but the surface integral over the curvature, Eq. (9) cannot be performed analytically and a complete closed expression cannot be obtained. Hence we choose to numerically evaluate all the dynamic and geometric cumulants. The behavior of the two dynamic cumulants ($n = 1, 2$) are shown in Figs. 2(a) and 2(b) for equal initial temperatures. The qualitative behavior is not that different from the undriven case apart from change in magnitude and the saturating values are also the equal to what was earlier observed for nondriven case [51]. These also retain the symmetry (antisymmetry) of the even (odd) cumulants with respect to the exchange of the left and right squeezing parameters under equal initial temperature ($T_\ell^o = T_r^o$) setting as well as the saturating behavior as observed earlier for undriven case [51]. The solid lines in Fig. 2 are evaluated by keeping x_r fixed while x_ℓ is varied. The dotted lines represent the case when $x_\ell \rightarrow x_r$ while x_ℓ is varied. This is simply because the rates that affect the dynamic cumulants are just scaled by the hyperbolic cosine functions [Eq. (3) and Eq. (4)] and does not alter the overall mathematical structure of the eigenvalue $\zeta_o(\lambda, t)$ [Eq. (A14)]. In the figures, we also have denoted the cumulants in absence of squeezing ($x_v = 0$) and driving as $j_o^{(n)}$ by defining a dimensionless ratio $C_{d/g}^{(n)} := j_{d/g}^{(n)} / j_o^{(n)}$. When $|C_{d/g}^{(n)}| > (<) 1$, the squeezing increases (decreases) the value

of the cumulant in comparison to the unsqueezed and undriven case.

On substituting the left and right eigenvectors of $\check{L}(\lambda, t)$ in the geometricity term $\langle L(\lambda, t) | \check{R}(\lambda, t) \rangle$ of Eq. (8) we can identify the geometric flux and geometric noise. The geometric flux is given by,

$$j_g^{(1)} = -\frac{\Omega}{2\pi} \int_0^{t_p} \frac{2\Gamma \cosh(2x_\ell) \cosh(2x_r)}{(\gamma_\ell X_\ell^+ + \gamma_r X_r^+)^3} dt \quad (10)$$

and shown in Fig. 2(c). Note that the geometric flux decays to zero at higher values of the squeezing parameter. The geometric noise is given by

$$j_g^{(2)} = -\frac{\Omega}{2\pi} \int_0^{t_p} \frac{12\Gamma^2 \cosh(2x_\ell) \cosh(2x_r) (X_r^+ - X_\ell^+)}{(\gamma_\ell + \gamma_r)(\gamma_\ell X_\ell^+ + \gamma_r X_r^+)^5} dt \quad (11)$$

with $\Gamma = \gamma_\ell \gamma_r (\gamma_\ell + \gamma_r)$ and $X_v^\pm := \cosh(2x_v) [2n_v(t) \pm 1]$. The RHS of Eq. (10) and Eq. (11) are evaluated as a function of the squeezing parameters and the scaled function is shown in Fig. 2(c) and Fig. 2(d), respectively. Both the geometric cumulants are observed decaying to zero as the squeezing parameters are increased. However, intermediate squeezing [peak and dip region in Fig. 2(d)] amplifies the geometric noise to a much larger extent (several orders of magnitude) than the dynamic noise, Fig. 2(b). Further, it is also observed that the geometric flux (odd cumulant) is symmetric with respect to exchanging the squeezing parameters while the second cumulant is antisymmetric, contrary to the behavior of the dynamic cumulants. The symmetric behavior upon exchanging x_ℓ and x_r in the geometric flux is because the denominator in the integrand inside the RHS of Eq. (10) is symmetric with respect to exchange. The noise is antisymmetric with respect to exchange because the numerator the RHS of Eq. (10) imparts a negative sign upon exchanging the squeezing parameters. It is interesting to note that both the exchange symmetry and the antisymmetry does not hold when the initial temperatures are different. This is shown graphically in Figs. 3(a) and 3(b). Note that, in Eq. (11), when $X_r^+ = X_\ell^+$, we obtain $j_g^{(2)} = 0$. This condition can be triggered by controlling the squeezing parameters x_ℓ and x_r and can be seen as the zero line along the diagonal ($x_\ell = x_r$) of the contour plot in Fig. 3(c). Under this same condition $X_r^+ = X_\ell^+$, the integral in Eq. (10) is, however, nonzero and hence one observes geometric flux [Fig. 3(d)]. We conclude that that when $X_r^+ = X_\ell^+$, we observe geometric flux but not the geometric noise.

We now move on to explain why the geometric effects in the flux and fluctuations vanish at higher squeezing values as seen in Figs. 2(c), 2(d) and Fig. 3. This is because $S_g(\lambda)$ vanishes at higher values of x_ℓ, x_r , as seen in Fig. 1(d). The geometric curvature, in the present model, can be known by evaluating the standard known expression of the geometric curvature [7, 11, 12],

$$\mathcal{F}_{T_\ell T_r} = \langle \partial_{T_\ell} L_o(\lambda) | \partial_{T_r} R_o(\lambda) \rangle - \langle \partial_{T_r} L_o(\lambda) | \partial_{T_\ell} R_o(\lambda) \rangle. \quad (12)$$

By substituting the left and right eigenvectors of $\check{L}(\lambda, t)$ (see the Appendix) in the above expression, we obtain after some

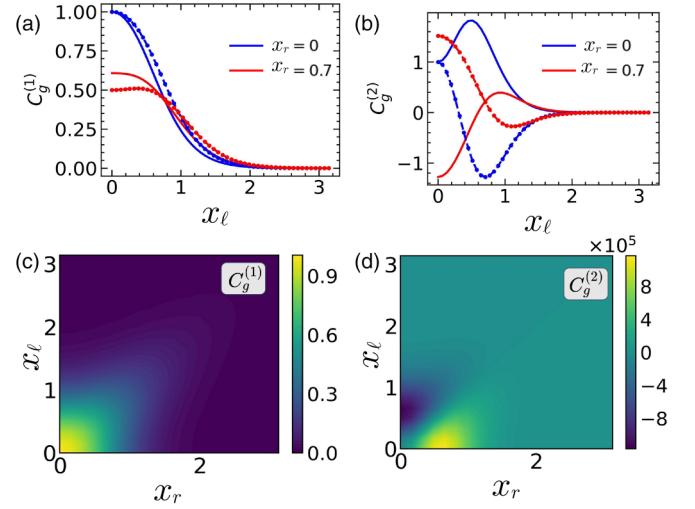


FIG. 3. Plot highlighting absence of symmetry and antisymmetry in the (a) geometric flux and (b) noise under unequal initial temperatures upon exchanging the squeezing parameters. The solid (dotted) lines are when x_r is fixed at 0 and 0.7 and x_ℓ is varied [x_ℓ and x_r are exchanged in Eq. (7)]. Contour plots showing the vanishing (c) geometric flux and (d) noise at higher values of squeezing parameters. Note the zero values along the diagonal.

algebra,

$$F_{T_\ell T_r}(\lambda) = -\frac{2\Gamma C_\ell C_r \sin(\lambda)}{\{K + 4f(\lambda)\}^{3/2}} \quad (13)$$

with

$$C_v = \frac{\hbar\omega_o e^{\hbar\omega_o/k_B T_v}}{k_B T_v^2} \left((n_v + 1/2) \cosh(2x_v) - \frac{1}{2} \right)^2 \quad (14)$$

$$K = \sum_{v=\ell, r} 2\gamma_v \cosh(2x_v) \left(n_v + \frac{1}{2} \right) \quad (15)$$

$$f(\lambda) = \prod_{v=\ell, r} \gamma_v (\cosh(2x_v) (n_v + 1/2) - 1/2) \times (e^{\hbar\omega_o/k_B T_\ell} (e^\lambda - 1) + e^{\hbar\omega_o/k_B T_r} (e^{-\lambda} - 1)) \quad (16)$$

and is analogous to the known expression for the unsqueezed case ($x_v = 0$) [51]. $F_{T_\ell T_r}(\lambda)$ is finite for the unsqueezed case around $\lambda = 0$. At low values of λ , the $\sin(\lambda)$ dominates over the denominator's $f(\lambda)$ term resulting in the typical modified sinusoidal shape as already reported. In the present case too, at lower values of squeezing ($x_\ell, x_r \approx 0$) around $\lambda = 0$, such a behavior is shown for $S_g(\lambda)$ as shown in Fig. 1(d). As x_v is increased, the hyperbolic terms from the squeezing parameters start contributing more to Eq. (13) around $\lambda = 0$ and changes the overall geometricity. These squeezed parameters can now be used to gain control or steer the underlying geometric statistics.

Note that, in general, the mathematical structure of $F_{T_\ell T_r}$ in Eq. (13) is such that the numerator (denominator) has an overall squared (cube-halved) dependence on the cosine hyperbolic terms. This structure dictates that as one keeps squeezing the reservoirs the denominator keeps increasing and hence the amplitude (quantified by the coefficients) of the $\sin(\lambda)$ term keeps reducing, which results in lower slope

around $\lambda = 0$. This causes the geometric flux and subsequent cumulants to keep reducing and finally vanishes as shown in Fig. 1(d). We can safely conclude that squeezing the reservoirs reduces the geometricity of the driven system. In this high-squeezing limit, even upon increasing the frequency of phase-different driving, $\Omega \gg 1$, the statistics of exchange is solely governed by the dynamicity of the system, i.e., $S_d(\lambda)$. We can prove this analytically by considering the following limiting case. Under the assumption that $n_v \ll 1/2$ (low-temperature regime), we have,

$$C_v|_{n_v \ll 1/2} \propto \cosh(2x_v) - 1 \quad (17)$$

$$K|_{n_v \ll 1/2} \propto \sum_v \cosh(2x_v) \quad (18)$$

$$f(\lambda)|_{n_v \ll 1/2} \propto \prod_v [\cosh(2x_v) - 1], \quad (19)$$

which results in

$$F_{T_\ell T_r}|_{n_v \ll 1/2} \propto \frac{\sin(\lambda)}{\sqrt{\sum_v \cosh^3(2x_v)} \sqrt{\prod_v [\cosh(2x_v) - 1]}}. \quad (20)$$

In the above expression, taking either of the two limits, $x_\ell \rightarrow \infty$ or $x_r \rightarrow \infty$ results in the RHS being zero. Thus, squeezing the reservoirs to its extremum kills the geometric curvature or the geometricity resulting in $S_g(\lambda) = 0$. The complete contour plots of the two geometric cumulants $C_g^{(1)}$ and $C_g^{(2)}$ as a function of x_ℓ and x_r are shown in Figs. 3(c) and 3(d). In both the plots, the geometric effects vanish at higher values of squeezing.

IV. THERMODYNAMIC UNCERTAINTY RELATIONSHIP

For an undriven case, $j_g^{(n)} = 0$ (when $\Omega = 0$ or $\phi = 0$), a standard thermodynamic uncertainty relationship (TUR), reminiscent of a steady-state fluctuation theorem holds, given by $F\mathcal{A} \geq 2k_B$ [45,52] with $F = j^{(2)}/j^{(1)}$ being the Fano factor while \mathcal{A} is the thermodynamic affinity of the system. This TUR has been shown not to hold in the presence of geometric effects [14].

In the present case, one can recover the standard TUR in the high-squeezing limit of either reservoir. Under maximum squeezing, $F_{T_\ell T_r}(\lambda) = 0$ kills the geometric contributions to the system statistics. We can hence recover a Gallavotti-Cohen symmetry,

$$\lim_{x_v \rightarrow \infty} \frac{1}{t_p} \int_0^{t_p} \zeta_o(\lambda, t) dt = \lim_{x_v \rightarrow \infty} \frac{1}{t_p} \int_0^{t_p} \zeta_o(-\lambda - \lim_{x_v \rightarrow \infty} \mathcal{A}, t) dt, \quad (21)$$

with the current model's thermodynamic affinity being

$$\mathcal{A} = \log \left(\frac{\int_0^{t_p} X_\ell^- X_r^+ dt}{\int_0^{t_p} X_\ell^+ X_r^- dt} \right), \quad (22)$$

where the time- and squeezing-dependent quantities X_v^\pm are defined in the text below Eq. (11). Equation (22) reduces to the known expression $1/T_\ell - 1/T_r$ in absence of driving [7] that leads to a steady-state fluctuation theorem. The recovery

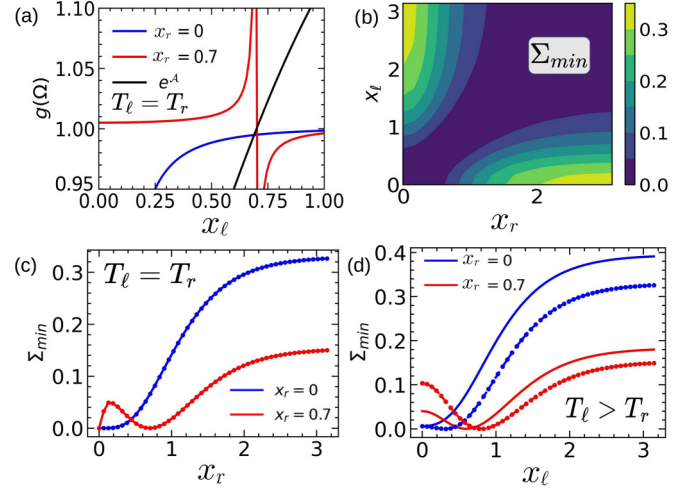


FIG. 4. (a) Behavior of the geometric correction factor, $g(\Omega)$ to the TUR as a function of x_ℓ for $x_r = 0, 0.7$. Note the singularity at $x_\ell = 0.7, x_r = 0.7$ at equal temperature (derivative shaped curve). At this value of x_ℓ , the thermodynamic force, $\mathcal{A} = 0$ [slanted line is $\exp(\mathcal{A})$]. For $x_r = 0$, there is no singularity (the curve bounded below unity). (b) Contour of Σ_{\min} as a function of squeezing parameters. The region where it is zero is where $\mathcal{A} = 0$. (c) Symmetry in the minimum entropy upon exchanging the values of the squeezing parameters. (d) Behavior of the minimum entropy produced as a function of x_ℓ at unequal temperature for $x_r = 0, 0.7$. It is zero at $x_\ell = x_r$. The solid (dotted) lines are when x_r is fixed at 0 and 0.7 and x_ℓ is varied [x_ℓ and x_r are exchanged in Eq. (7)].

of the symmetry hence allows us to recover the standard TUR,

$$\lim_{x_v \rightarrow \infty} \mathcal{A} \frac{\lim_{x_v \rightarrow \infty} j_d^{(2)}}{\lim_{x_v \rightarrow \infty} j_d^{(1)}} \geq 2k_B. \quad (23)$$

In the case of finite (but not maximal) squeezing, the geometricities are still present. TUR in such a case has been shown to get modified by including a geometric correction factor [18],

$$\frac{j^{(2)}\Sigma}{(j^{(1)})^2 g(\Omega)} \geq 2k_B, \quad (24)$$

where, $g(\Omega)$ is the driving-dependent geometric correction factor and is of the form,

$$g(\Omega) = \frac{1}{(1 + j_g^{(1)}/j_d^{(1)})^2}. \quad (25)$$

We numerically evaluate Eq. (25) and plot $g(\Omega)$ as a function of x_ℓ in Fig. 4(a) where a discontinuity is observed at $x_\ell = 0.7$. This discontinuity is at that point of x_ℓ , where $\mathcal{A} = 0$ ($e^{\mathcal{A}}$ is shown as a vertically slanted line) that results in $j_d^{(1)} = 0$ in Eq. (25). Further, for any fixed value of $j_g^{(1)}$ in Eq. (24), the RHS is greater (less) than unity when $j_d^{(1)} < (>) 0$ and vice versa. We have earlier shown that, for an undriven case, the direction of the dynamic flux $j_d^{(1)}$ is controllable through the squeezing parameters due to the modification of the thermodynamic affinity, \mathcal{A} [51]. Thus by controlling x_ℓ , we observe regions where $g(\Omega) > 1$ and $g(\Omega) < 1$ characterized by a shift between these two regions at that value of x_ℓ where

$\mathcal{A} = 0$ as seen in Fig. 4(a). The curve below unity is evaluated by maintaining positive geometric flux and $\mathcal{A} > 0$ ($T_\ell = T_r$, $x_\ell = 0.7$, $x_r = 0$) so that $g(\omega) < 1$. In a standard context without squeezing, as in the work of Lu *et al.* [18] where $g(\Omega)$ was introduced, the dynamic flux is solely dependent on the temperature gradient, which controls the thermodynamic affinity and the $g(\Omega)$ is a continuous function either below unity or above unity depending on the signs of the dynamic or geometric fluxes.

We state that the observed discontinuity in the behavior of $g(\Omega)$ in Fig. 4(a) does not lead to violation of the modified TUR, Eq. (24). Although, not highlighted in the earlier work [18], the continuity of $g(\Omega)$ in Eq. (24) as a function of a system parameter is rather limited to the sign of the ratio of the two fluxes, $j_g^{(1)}/j_d^{(1)}$ in the denominator of Eq. (25). For positive dynamic flux (characterized by $\mathcal{A} > 0$) or geometric flux, the correction factor $g(\Omega) < 1$, since the denominator of Eq. (25) is always greater than unity. For either negative dynamic flux ($\mathcal{A} < 1$) or geometric flux, the denominator of Eq. (25) is less than unity resulting in $g(\Omega) > 1$. So whenever there is sign change in either of the two fluxes, $j_d^{(1)}$ or $j_g^{(1)}$, as a result of system parameter change (by tuning ϕ , x_ℓ , x_r , etc.), $g(\Omega)$ changes its behavior so that the TUR, Eq. (24) gets preserved. In Fig. 4(a), the discontinuity observed at $x_\ell = 0.7$ is that point of x_ℓ , where $j_d^{(1)}$ changes its sign (\mathcal{A} changes from less than unity to greater than unity) resulting in the change of behavior of $g(\Omega)$ from greater than unity to less than unity and preserving the TUR, Eq. (24).

As long as we maintain $\mathcal{A} > 0$, by properly choosing x_ℓ and x_r values, the modified TUR given by Eq. (24) always holds within these two separate regimes of $g(\Omega)$. Within the limit of adiabatic driving (with fast dephasing [7,53]), the Liouvillian of the reduced system, Eq. (24) is completely positive and trace preserving and obeys the detailed balance even with squeezed reservoirs, being of the Lindblad type [53,54]. Since the recently proposed TUR is found to be valid, we directly use it to estimate the entropy production, albeit its extremum value. By maintaining, $\mathcal{A} > 0$, we directly estimate the minimum entropy production, Σ_{\min} in the presence of geometricities by taking the equality at the minimum value of the entropy from Eq. (24),

$$\Sigma_{\min} = 2k_B \frac{(j_d^{(1)} + j_g^{(1)})^2}{j_d^{(2)} + j_g^{(2)}} g(\Omega). \quad (26)$$

In the above equation, it is not possible to separate the entropy rates into dynamic and geometric contributions. Although when $\Omega \gg 1$, $j_g^{(1)} \gg j_d^{(1)}$, the same cannot be said for the second cumulant, which makes the denominator in Eq. (26) to have combined dynamic and geometric contributions. Nonetheless, the modified TUR allows an easy way to evaluate the total minimum entropy production rate. Note that in the presence of geometricities, evaluation of entropies with contribution from both dynamic and geometric components is not at all straightforward [55] due to production of excess entropies. We evaluate Eq. (26) and plot it as a function of the left reservoir's squeezing parameters in Figs. 4(b)–4(d). The dependence of Σ_{\min} on x_ℓ is nonlinear and saturates at higher values. In Fig. 4(b), we show a contour map of Σ_{\min} for a wide range of x_ℓ and x_r values. There exists a wide region

of Σ_{\min} around the diagonal of the contour is where $\mathcal{A} \approx 0$ that results in $\Sigma_{\min} = 0$. This region is actually not allowed since $g(\Omega)$ is strictly not defined when $\mathcal{A} = 0$. One should not substitute this zero value of the minimum entropy in Eq. (24) and claim it as a violation of the TUR. In Fig. 4(c), we show the existence of the exchange symmetry between x_ℓ and x_r in the entropy under equal temperature setting. In Fig. 4(d), we show the absence of the exchange symmetry when the temperatures are unequal.

V. CONCLUSION

We employ a full counting statistical method to derive a tilted driven quantum master equation for a simple bosonic site coupled to two squeezed harmonic reservoirs. The temperatures of the two squeezed reservoirs are assumed to be adiabatically driven with a phase-different driving protocol. This allowed us to explore the combined effect of squeezing parameters and the geometricities or geometric phaselike contributions to the steady-state observables, the flux (first cumulant), and the noise (second cumulant). The dynamic cumulants exhibit similar qualitative behavior as a function of squeezing parameters to that of what is already known for an undriven scenario, albeit with modified magnitudes. The geometric cumulants are, however, affected by the squeezing parameters. The odd (even) geometric cumulants are found to be antisymmetric (symmetric) with respect to exchanging the left and right squeezing parameters when the initial thermal gradient is maintained at zero. These also decay to zero as we keep increasing the strength of the reservoirs' squeezing parameters. This is because an increased squeezing prohibits the generation of geometricity in the cumulant generating function. Hence, under maximum squeezing, one can recover a standard steady-state fluctuation theorem, which also leads to a standard thermodynamic uncertainty relation even in the presence of phase-different driving protocol. Using a recently proposed modified geometric thermodynamic uncertainty principle, which is robust in the presence of squeezing, we estimate the minimum entropy production rate at finite values of dynamic flux. This minimum entropy production rate cannot be separated into dynamic and geometric contributions. It exhibits a saturating behavior and is also symmetric with respect to exchange of the left and right squeezing parameters under a zero initial thermal gradient scenario.

ACKNOWLEDGMENTS

H.P.G. acknowledge the support from the University Grants Commission, New Delhi for the startup research grant, UGC(BSR), Grant No. F.30-585/2021(BSR) and the Science and Engineering Research Board for the startup grant with file number SERB/SRG/2021/001088.

APPENDIX

The Hamiltonian of the bare site interacting with two bosonic reservoirs can be written as,

$$\hat{H} = \hbar\omega_o \hat{b}^\dagger \hat{b} + \sum_{i=v, \nu \in L, R} \hbar\omega_i \hat{a}_i^\dagger \hat{a}_i + \hat{V}, \quad (A1)$$

with

$$\hat{V} = \sum_{i,v \in L,R} k_i^v (\hat{a}_{iv}^\dagger \hat{b} + \hat{a}_{iv} \hat{b}^\dagger). \quad (\text{A2})$$

Here, $\hbar\omega_o \hat{b}^\dagger \hat{b}$ is the on-site Hamiltonian with bare frequency ω_o , while \hat{b}^\dagger (\hat{b}) is the bosonic creation (annihilation operator) on the site. The second term is the reservoir Hamiltonian with squeezed harmonic states and is a sum of two terms that represent the left (L) and right (R) squeezed reservoirs. The single-particle operators \hat{a}_{iv}^\dagger (\hat{a}_{iv}) represent the creation (annihilation) of a boson in the i th mode from (of) the v th bath. \hat{V} is the system bath coupling Hamiltonian with k_i^v being the coupling constant for the i th squeezed mode of the v th bath to the bare site mode. The squeezed density matrix for the v th reservoir (\hat{H}_v being the v th reservoir Hamiltonian) is given by

$$\hat{\rho}_v = \frac{1}{Z} \exp\{-\beta_v(t) \hat{S}_v \hat{H}_v \hat{S}_v^\dagger\}, \quad (\text{A3})$$

$$\hat{S}_v = \prod_k e^{\frac{1}{2}(x_v^* \hat{a}_{kv}^2 - \text{H.c.})}, \quad (\text{A4})$$

$\beta_v(t) = [k_B T_v(t)]^{-1}$ being the inverse temperature and \hat{S}_v is the squeezing operator on the k th mode of the v th bath, with x_v being the squeezing the v th reservoir's squeezing parameter [27,48,51,56]. In accordance with standard perturbation theory framework [7,48,51] and considering interactions upto second order in the system-bath coupling, \hat{V} , the reduced system dynamics is given by:

$$\dot{\hat{\rho}} = -tr_B \int_0^t ds [\rho_T(t) \tilde{V}(t) \tilde{V}(s) - \tilde{V}(t) \tilde{\rho}_T(t) \tilde{V}(s) + \text{H.c.}], \quad (\text{A5})$$

where $t_s := t - s$ and $s = t - s$. The interaction picture is $\tilde{O}(t) = \exp(i\hat{H}_o t) \hat{O} \exp(-i\hat{H}_o t)$ where \hat{H}_o contains only the diagonal part from Eq. (A1). For any external modulations that give an extra time dependence to system parameters, a quantum master equation can be derived under some standard assumptions [9,12,17,57]. We restrict ourselves to modulations of the temperatures of the bath, which makes the bath density matrix time dependent. Assuming that the initial density matrix is factorizable, we can write $\tilde{\rho}_T(t) := \tilde{\rho}_l \otimes \rho_B$, with $\rho_B := \rho_L(t) \otimes \rho_R(t)$, being the externally driven time-dependent squeezed density matrices for the left and right reservoirs, respectively. ρ_l is the time-dependent squeezed density matrix. Substituting the value of the operator \hat{V} in Eq. (A5), the integrands can be rewritten as,

$$\begin{aligned} \tilde{\rho}_l \rho_B \tilde{V}(t_s) \tilde{V}(t) &= k_{iv}^2 (\langle \tilde{a}_{iv}^\dagger(t_s) \tilde{a}_{iv}(t) \rangle \tilde{\rho}(\tilde{b}(t_s) \tilde{b}(t) + \tilde{b}(t_s) \tilde{b}^\dagger(t)) \\ &+ \langle \tilde{a}_{iv}(t_s) \tilde{a}_{iv}^\dagger(t) \rangle \tilde{\rho}(\tilde{b}(t_s) \tilde{b}^\dagger(t) + \tilde{b}^\dagger(t_s) \tilde{b}^\dagger(t))) \end{aligned} \quad (\text{A6})$$

$$\begin{aligned} \tilde{V}(t) \tilde{\rho}_l \rho_B \tilde{V}(t_s) &= k_{iv}^2 (\langle \tilde{a}_{iv}^\dagger(t) \tilde{a}_{iv}(t_s) \rangle (\tilde{b}(t) \tilde{\rho} \tilde{b}(t_s) + \tilde{b}(t) \tilde{\rho} \tilde{b}^\dagger(t)) \\ &+ \langle \tilde{a}_{iv}(t) \tilde{a}_{iv}^\dagger(t_s) \rangle (\tilde{b}(t) \tilde{\rho} \tilde{b}^\dagger(t_s) \\ &+ \tilde{b}^\dagger(t) \tilde{\rho} \tilde{b}^\dagger(t_s))), \end{aligned} \quad (\text{A7})$$

where $\langle \cdot \rangle$ represents trace over the externally driven time-dependent squeezed density matrix. On evaluating the matrix elements of Eqs. (A6) and (A7), $\langle m | \cdot | n \rangle$, $m, n = 1, 0$, the terms with conjugate system operators survive leading to only $m = n$ terms. The nonzero squeezed bath expectation values are given by [48],

$$\langle \tilde{a}_{iv}^\dagger \tilde{a}_{iv} \rangle = \left(\cosh(2x_{iv})(n_v(t) + \frac{1}{2}) - \frac{1}{2} \right) f(t, s) \quad (\text{A8})$$

$$:= N_v(t) f(t, s) \quad (\text{A9})$$

$$\langle \tilde{a}_{iv}(t) \tilde{a}_{iv}^\dagger \rangle = \left(\cosh(2x_{iv})(n_v(t) + \frac{1}{2}) + \frac{1}{2} \right) f(t, s) \quad (\text{A10})$$

$$:= (1 + N_v(t)) f(t, s). \quad (\text{A11})$$

$n_v(t)$ is the Bose function for the v th externally driven time-dependent squeezed bath and $f(t, s) = \exp(it_s \omega_{iv}) \exp(-it \omega_{iv})$. On the assumption that only the thermodynamic equilibrium of the bath changes with time due to external driving, we obtain three time scales: internal baths' relaxation (t_B), system relaxation (t_s) due to coupling with the baths, and the time scale (t_d) of the external driving. We further assume that $t_B \ll t_s \ll t_d$, so that the Born approximation is valid so that modulation occurs under the adiabatic limit. With these definitions, a standard Born-Markov approximation ($t \rightarrow \infty$) within the wide-band limit coupled with the fast dephasing separated time-scale approximations [7,12,18,53,57], we can evaluate the time integrands in Eqs. (A6) and (A7) by substituting in Eq. (A5). The wide band limit normalizes the squeezing parameter of the k th mode of the v th bath, x_{iv} to a real positive number x_v [48] and also allows us to convert the coupling terms to a real positive constant γ_v . We can hence write down two adiabatic Pauli-type master equations, with time-dependent squeezed rates,

$$\begin{aligned} \dot{\rho}_{11} &= -(\gamma_L(1 + N_L(t)) + \gamma_R(1 + N_R(t)))\rho_{11} \\ &+ (\gamma_L N_L(t) + \gamma_R N_R(t))\rho_{00} \end{aligned} \quad (\text{A12})$$

$$\begin{aligned} \dot{\rho}_{00} &= (\gamma_L(1 + N_L(t)) + \gamma_R(1 + N_R(t)))\rho_{11} \\ &- (\gamma_L N_L(t) + \gamma_R N_R(t))\rho_{00}, \end{aligned} \quad (\text{A13})$$

where $\langle m | \rho | m \rangle = \rho_{mm}$ represents the probability of occupation of the occupied and unoccupied Fock states. Note that the populations and coherences are decoupled and the equations are effectively classical albeit with quantum mechanical rates [58]. Now we can recast the above two equations in the Liouville space and following the standard procedure of FCS by introducing the auxiliary counting field, λ to keep track of the net number of bosons exchanged, q (between left reservoir and system) [41,47], we can define the time-dependent moment generator, Eq. (2), where the quantum mechanical rates have been redefined to $\alpha_v(t) = \gamma_L[1 + N_L(t)]$ and $\beta_v = \gamma_v N_v(t)$. The λ -dependent zero eigenvalue of Eq. (2) is given

by,

$$\zeta_o(\lambda, t) = -(\gamma_\ell X_\ell^+ + \gamma_r X_r^+) + \sqrt{(\gamma_\ell + \gamma_r)^2 + (\gamma_\ell X_\ell^- + \gamma_r X_r^-)} f(\lambda) \quad (\text{A14})$$

$$X_v^\pm = \cosh(2x_v)(2n_v(t) \pm 1), \quad v = l, r \quad (\text{A15})$$

$$f(\lambda) = [\gamma_\ell e^{-\lambda}(1 + X_\ell^+) + \gamma_r e^{2\lambda}(X_r^+)] \quad (\text{A16})$$

from which the dynamic flux and noise can be numerically evaluated using Eq. (7). The left and the right eigenvectors of $\check{\mathcal{L}}(\lambda, t)$ are obtained as,

$$|R_\pm(\lambda, t)\rangle = \{u_\pm, 1\} \quad (\text{A17})$$

$$\langle\langle L_\pm(\lambda, t) | = \frac{1}{u_+(t) - u_-(t)} \{\pm 1, \mp u_\mp(t)\}, \quad (\text{A18})$$

with

$$u_\pm(t) = \sum_{v=L,R} \frac{-[\alpha_v(t) + \beta_v(t)] \pm \sqrt{[\alpha_v(t) - \beta_v(t)]^2 + 4\alpha_\lambda(t)\beta_\lambda(t)}}{2\alpha_\lambda(t)}. \quad (\text{A19})$$

Here, $\alpha_\lambda = \alpha_l e^{-\lambda} + \alpha_r$, $\beta_\lambda = \beta_l e^\lambda + \beta_r$. The + subscript in the eigenvectors corresponds to the zero eigenvalue (the largest eigenvalue), ζ_o , which we denoted in the paper as L_o

or R_o . Substituting these values in the Eqs. (7)–(9) allows us to arrive at Eq. (10), (11), and (12) after some algebraic simplifications.

-
- [1] S. Pancharatnam, *Proc. Indian Acad. Sci. A* **44**, 247 (1956).
 [2] M. V. Berry, *Proc. Roy. Soc. Lond. A* **392**, 45 (1984).
 [3] N. Mukunda and R. Simon, *Ann. Phys. (NY)* **228**, 205 (1993).
 [4] D. J. Thouless, *Phys. Rev. B* **27**, 6083 (1983).
 [5] A. Carollo, I. Fuentes-Guridi, M. F. Santos, and V. Vedral, *Phys. Rev. Lett.* **90**, 160402 (2003).
 [6] Z. Wang, L. Wang, J. Chen, C. Wang, and J. Ren, *Front. Phys.* **17**, 1 (2022).
 [7] J. Ren, P. Hänggi, and B. Li, *Phys. Rev. Lett.* **104**, 170601 (2010).
 [8] S. K. Giri and H. P. Goswami, *Phys. Rev. E* **106**, 024131 (2022).
 [9] Y. Hino and H. Hayakawa, *Phys. Rev. E* **102**, 012115 (2020).
 [10] K. Takahashi, Y. Hino, K. Fujii, and H. Hayakawa, *J. Stat. Phys.* **181**, 2206 (2020).
 [11] N. Sinitsyn and I. Nemenman, *Europhys. Lett.* **77**, 58001 (2007).
 [12] H. P. Goswami, B. K. Agarwalla, and U. Harbola, *Phys. Rev. B* **93**, 195441 (2016).
 [13] Y. Hino and H. Hayakawa, *Phys. Rev. Res.* **3**, 013187 (2021).
 [14] S. K. Giri and H. P. Goswami, *Phys. Rev. E* **96**, 052129 (2017).
 [15] S. K. Giri and H. P. Goswami, *Phys. Rev. E* **99**, 022104 (2019).
 [16] J. Eglinton and K. Brandner, *Phys. Rev. E* **105**, L052102 (2022).
 [17] T. Yuge, T. Sagawa, A. Sugita, and H. Hayakawa, *Phys. Rev. B* **86**, 235308 (2012).
 [18] J. Lu, Z. Wang, J. Peng, C. Wang, J.-H. Jiang, and J. Ren, *Phys. Rev. B* **105**, 115428 (2022).
 [19] D. F. Walls, *Nature (London)* **306**, 141 (1983).
 [20] R. Schnabel, *Phys. Rep.* **684**, 1 (2017).
 [21] V. Dodonov, A. Klimov, and V. Man'ko, *Group Theoretical Methods in Physics* (Springer, Berlin, 1991).
 [22] R. Puri, *pramana* **48**, 787 (1997).
 [23] L. Dupays and A. Chenu, *Quantum* **5**, 449 (2021).
 [24] T. Abebe, D. Jobir, C. Gashu, and E. Mosisa, *Adv. Math. Phys.* **2021**, 6696253 (2021).
 [25] A. Kumar, S. Lahiri, T. Bagarti, and S. Banerjee, *Physica A* **623**, 128832 (2023).
 [26] Z. Holmes, S. Weidt, D. Jennings, J. Anders, and F. Mintert, *Quantum* **3**, 124 (2019).
 [27] H. K. Yadalam, B. K. Agarwalla, and U. Harbola, *Phys. Rev. A* **105**, 062219 (2022).
 [28] G. Manzano, F. Galve, R. Zambrini, and J. M. R. Parrondo, *Phys. Rev. E* **93**, 052120 (2016).
 [29] W. Niedenzu, D. Gelbwaser-Klimovsky, A. G. Kofman, and G. Kurizki, *New J. Phys.* **18**, 083012 (2016).
 [30] B. K. Agarwalla, J.-H. Jiang, and D. Segal, *Phys. Rev. B* **96**, 104304 (2017).
 [31] J. Klaers, S. Faelt, A. Imamoglu, and E. Togan, *Phys. Rev. X* **7**, 031044 (2017).
 [32] D. Newman, F. Mintert, and A. Nazir, *Phys. Rev. E* **95**, 032139 (2017).
 [33] A. Ourjoumtsev, A. Kubanek, M. Koch, C. Sames, P. W. Pinkse, G. Rempe, and K. Murr, *Nature (London)* **474**, 623 (2011).
 [34] M. Mehmet, H. Vahlbruch, N. Lastzka, K. Danzmann, and R. Schnabel, *Phys. Rev. A* **81**, 013814 (2010).
 [35] X. L. Huang, T. Wang, and X. X. Yi, *Phys. Rev. E* **86**, 051105 (2012).
 [36] J.-T. Hsiang and B.-L. Hu, *Ann. Phys. (NY)* **433**, 168594 (2021).
 [37] P. Talkner, M. Morillo, J. Yi, and P. Hänggi, *New J. Phys.* **15**, 095001 (2013).
 [38] C. Wang, H. Chen, and J.-Q. Liao, *Phys. Rev. A* **104**, 033701 (2021).
 [39] F. Giraldi and F. Petruccione, *Eur. Phys. J. D* **68**, 1 (2014).
 [40] J. P. Pekola and B. Karimi, *Rev. Mod. Phys.* **93**, 041001 (2021).
 [41] M. Esposito, U. Harbola, and S. Mukamel, *Rev. Mod. Phys.* **81**, 1665 (2009).
 [42] D. Segal and A. Nitzan, *Phys. Rev. E* **73**, 026109 (2006).
 [43] P. Carpio-Martinez and G. Hanna, *J. Chem. Phys.* **154**, 094108 (2021).
 [44] A. Kowalewska-Kudlaszyk and R. Tanaś, *J. Mod. Opt.* **48**, 347 (2001).

- [45] S. Saryal, H. M. Friedman, D. Segal, and B. K. Agarwalla, *Phys. Rev. E* **100**, 042101 (2019).
- [46] Y. Lu, N. Lambert, A. F. Kockum, K. Funo, A. Bengtsson, S. Gasparinetti, F. Nori, and P. Delsing, *PRX Quantum* **3**, 020305 (2022).
- [47] U. Harbola, M. Esposito, and S. Mukamel, *Phys. Rev. B* **76**, 085408 (2007).
- [48] S.-W. Li *et al.*, *Phys. Rev. E* **96**, 012139 (2017).
- [49] R. Tanas, *J. Opt. B: Quantum Semiclassical Opt.* **4**, S142 (2002).
- [50] Y. Zou, Y. Jiang, Y. Mei, X. Guo, and S. Du, *Phys. Rev. Lett.* **119**, 050602 (2017).
- [51] M. J. Sarmah, A. Bansal, and H. P. Goswami, *Physica A* **615**, 128620 (2023).
- [52] P. Pietzonka, F. Ritort, and U. Seifert, *Phys. Rev. E* **96**, 012101 (2017).
- [53] D. Segal, *Phys. Rev. B* **73**, 205415 (2006).
- [54] G. De Chiara, G. Landi, A. Hewgill, B. Reid, A. Ferraro, A. J. Roncaglia, and M. Antezza, *New J. Phys.* **20**, 113024 (2018).
- [55] T. Yuge, T. Sagawa, A. Sugita, and H. Hayakawa, *J. Stat. Phys.* **153**, 412 (2013).
- [56] V. Dodonov, *J. Opt. B: Quantum Semiclassical Opt.* **4**, R1 (2002).
- [57] T. Albash, S. Boixo, D. A. Lidar, and P. Zanardi, *New J. Phys.* **14**, 123016 (2012).
- [58] D. A. Bagrets and Y. V. Nazarov, *Phys. Rev. B* **67**, 085316 (2003).